Ionization of Water as an Effect of Quantum Delocalization at Aqueous Electrode Interfaces

Jinggang Lan,* Vladimir Rybkin, and Marcella Iannuzzi*

Department of Chemistry, University of Zürich, Zürich

E-mail: jinggang.lan@chem.uzh.ch; marcella.iannuzzi@chem.uzh.ch

Phone: +41 44 63 544 79

Details of the DFT calculation and model

The electronic structure is described using PBE functional[1] with D3 correction[2] within the Gaussian and plane waves framework.[3] Molecular orbitals of the valence electrons are expanded into DZVP-MOLOPT-SR-GTH basis sets,[4] while atomic core electrons are described through Goedecker-Teter-Hutter (GTH) pseudopotentials.[5,6] The dipole correction scheme[7] has been applied along the Z direction.

The metal/water simulation cell system consists of a four-layer (6×6) (111) surface-slab in contact with 134 explicit water molecules. For Pt(111) it is an orthorhombic box of $14.93 \times 17.24 \times 50$ Å^3 size. In the case of Au(111) surface, the cell is $15.23 \times 17.59 \times 50$ Å^3. The simulations are carried out by keeping the two bottom metal layers constrained at the initial coordinates in order to maintain the bulk behavior of the inner part of the slab.

The orientation of a water molecule is defined in terms of the angle between the OH bond and the normal to the surface as shown in the Fig.1. This means that cosines close to +1 correspond to OH pointing outwards (to bulk), cosines around 0 correspond to OH parallel to the surface, and negative values indicate OH pointing towards the surface.
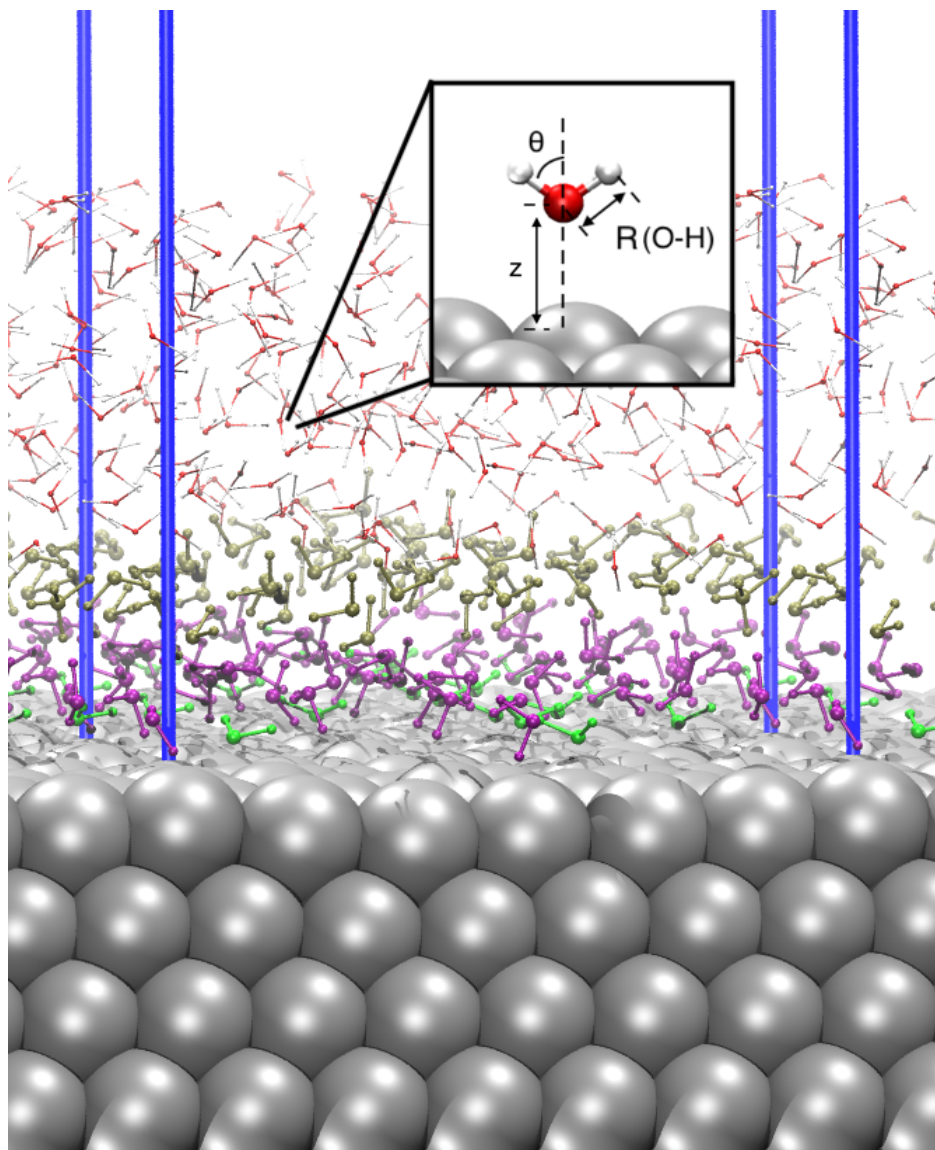
Supplementary Figure 1: Atomistic model representing Pt(111) slab in contact with liquid water. The blue lines delimit the simulation cell in periodic boundary conditions. Inset: graphical representation of OH bond length, OH orientation, and oxygen's z coordinate, as referred in the text. Color code: silver spheres are Pt atoms, red O atoms, and grey H atoms and the first three layers of water are labeled in green, purple and olive.

Convergence tests

In order to assess the model's reliability, convergence tests have been carried out on the electronic properties of the metallic surface. In particular, we compare the workfunctions as obtained from the 6×6 models, which are 5.80 eV for Pt and 5.20 eV for Au , with the ones obtained for the larger (or thicker models), which are around 5.70 eV (Pt) and 5.20 eV (Au) (See Table. 1). The projected densities of states of the topmost layer obtained for the different models are also compared , also demonstrating that the electronic properties are well reproduced also by the smaller model. (See Fig.2)
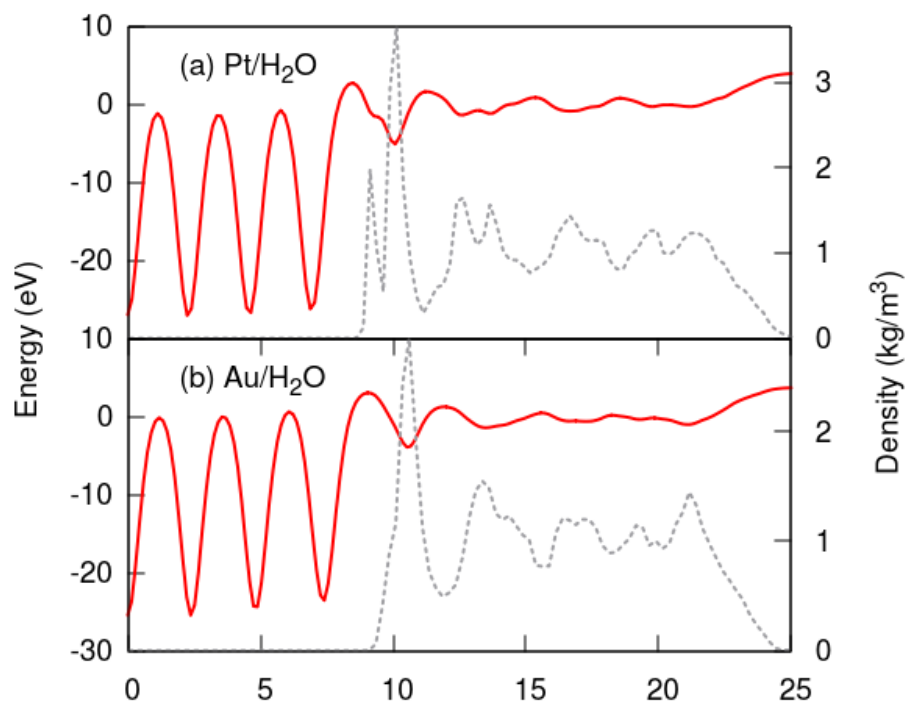
Table.1 Workfuntion (eV) as obtained from different slab models

	6x6-4-layer	8x8-4-layer	12x12-4-layer	8x8-6-layer
Pt-111	5.80	5.72	5.71	5.70
Au-111	5.20	5.24	5.20	5.13
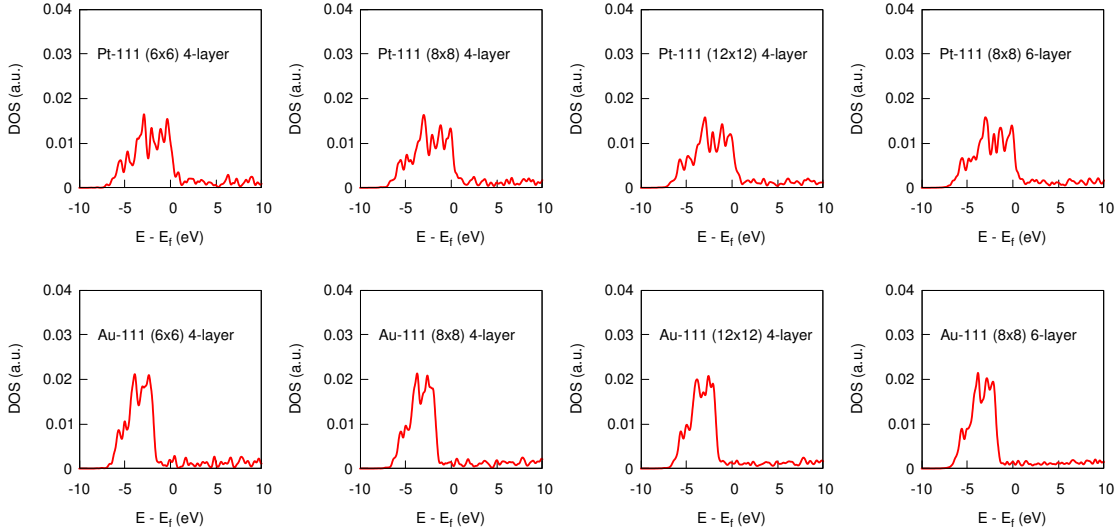
Supplementary Figure 2: Projected densities of states of the topmost layer obtained for the different models.

Hartree potential

Supplementary Figure 3: In plane averaged electrostatic potential across the (a) Pt/H$_2$O interface and (b) Au/H$_2$O. The plotted values correspond to the ensemble average over the the quantum trajectories. The dashed line represents the water's density.
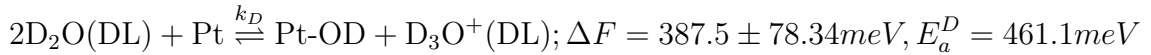
D₂O *vs* H₂O on platinum surfaces

Experimentally the impact of nuclear quantum effects can be determined by replacing the H by their heavier isotopes, i.e., revealing kinetic isotope effects. Indeed, it has been observed that the pH of liquid water increases from 7.0 to 7.4 upon deuteration. That is consistent with quasiharmonic scaling, since the pK_w varies as the inverse of the square root of the particle mass.[8] The extrapolated value to the classical limit, where the mass of hydrogen is infinite, is ∼8.5.[9] Similarly, when replacing hydrogen to deuterium in the simulation of the Pt/water interface, our approach reveals a significantly reduced probability to observe self-Ionization processes at the interface, which can be quantified by the evaluation of the relative pK_{eq} constants and corresponding kinetic energy barriers.

The free energy is estimated using the probability of the coordination number of oxygen:

$$F = -k_b T \ln P(\text{CN}_\text{O}) \tag{1}$$

For the process of $H_2O \rightarrow OH^-$ the CN_O change from 2 to 1 and $H_2O \rightarrow H_3O^+$ change from 2 to 3. The activation energy barrier are height of a potential barrier.

$$2H_2O(\text{DL}) + \text{Pt} \overset{k_H}{\rightleftharpoons} \text{Pt-OH} + H_3O^+(\text{DL}); \Delta F = 357.00 \pm 85.05 meV, E_a^H = 376.3 meV$$

$$2D_2O(\text{DL}) + \text{Pt} \overset{k_D}{\rightleftharpoons} \text{Pt-OD} + D_3O^+(\text{DL}); \Delta F = 387.5 \pm 78.34 meV, E_a^D = 461.1 meV$$

The rates can be estimated using path-integral transition state theory to estimate the isotopic kinetics:[10]

$$k_{H(D)} = \kappa \frac{k_B T}{h} exp(-\frac{E_a}{k_B T}) \tag{2}$$

where κ is the transmission coefficient, T is the temperature of 300K, k_B is the Boltzmann constant, h is the Planck's constant, and E_a is the activation energy. For simplicity, κ=1 is used and the recrossing is neglected.

The kinetic isotope effect ($K^{H/D}$) is defined as the ratio of rate constants for the self-Ionization of the light and the heavy water.

$$K^{H/D} = \frac{k_H}{k_D} = exp(\frac{E_a^D - E_a^H}{k_B T}) \tag{3}$$

Comparison between Aqueous platinum and gold surfaces

To assess the role of the surface electronic properties on the water dissociation process, we applied the same procedure to the $H_2O/Au(111)$ system. In this case, we do not observe the same enhancement of self-Ionization of water when NQEs are included. FIG.4. The N_{ion} never goes beyond 2 at the water-gold interface.
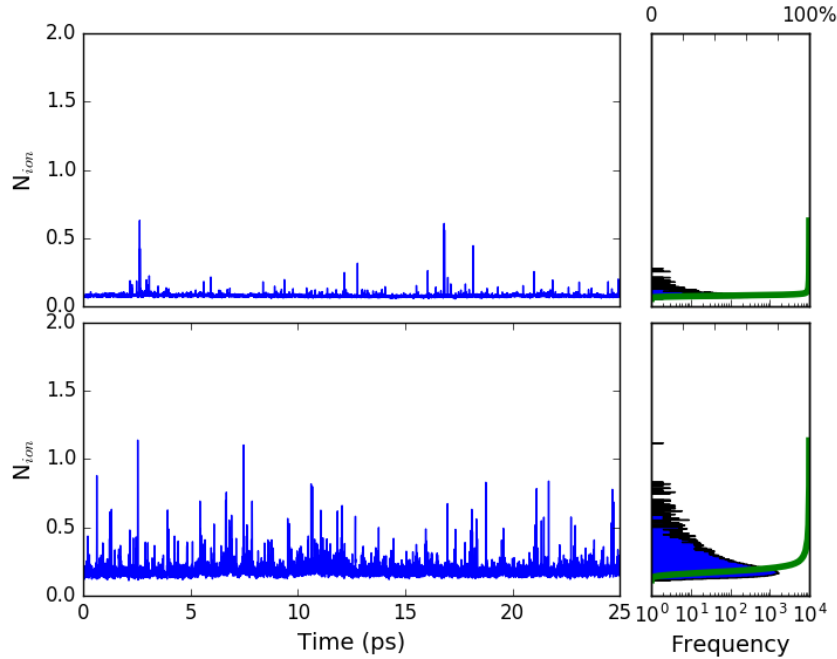
Supplementary Figure 4: N_{ion} parameter as obtained from $H_2O/Au(111)$ at each step of the AIMD and PI-AIMD trajectories, respectively. In the right panels the effective counting of observations for each N_{ion} value, presented in logarithmic scale. The green curve measures in cumulative percentage of the probability distribution.

The water density profiles across the interface as obtained by averaging over the clas-

sical as well as the quantum trajectories clearly present the substantial differences in the interaction with Pt and Au (FIG.5). On Au(111) we obtain a more compact slab, with a single broad first peak, which is centered at the position of the second layer of water on Pt(111). This is due to the weaker interaction of water to Au, which prevents the formation of a first layer of covalently bound molecules. Nevertheless, the density within the contact layer is higher than in the bulk, and this first layer is separated from the diffusion layer by a depletion region similar to what observed on Pt.
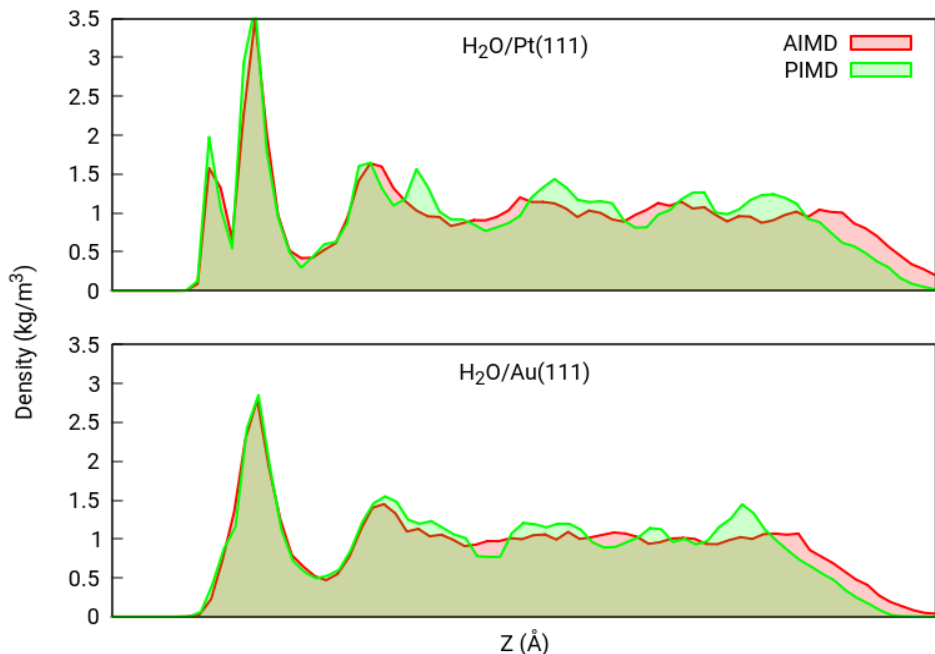

Supplementary Figure 5: Density profile of water across the interface with the metal as obtained from the ensemble average for the classical (red) and the quantum (green) sampling. The top panel is the profile at the Pt(111) interface and the bottom panel corresponds to Au(111).

In Fig.6, we compare the OH bond length distribution extracted from the classical and quantum trajectory as a function of the oxygen's height above the metal surface. As already discussed in the manuscript for the Pt(111) case, also on Au(111) the quantum hydrogens' delocalization induced the elongation of the OH bonds, also in the bulk water region. The more significant differences between the two metal interfaces are noticed close to the surface.

The less structured water arrangement at the Au(111) surface, already implied by the analysis of the density profile, is confirmed by both classical and quantum distributions. The double peak characterising the double layer at Pt(111) is replaced by a broader feature on Au(111), and the large fluctuations due to proton hopping events are not present. It turns out that NQEs contribute O-H prolongation almost equally in both interfacial and bulk water on Au surface. (see Fig.6) The molecules closer to the Au(111) surface still tend to be oriented with the OH outwards, as on Pt. However, the molecules at slightly larger distance, still belonging to the contact layer, are more isotropically oriented (FIG.7), confirming a less structured arrangement in this region.
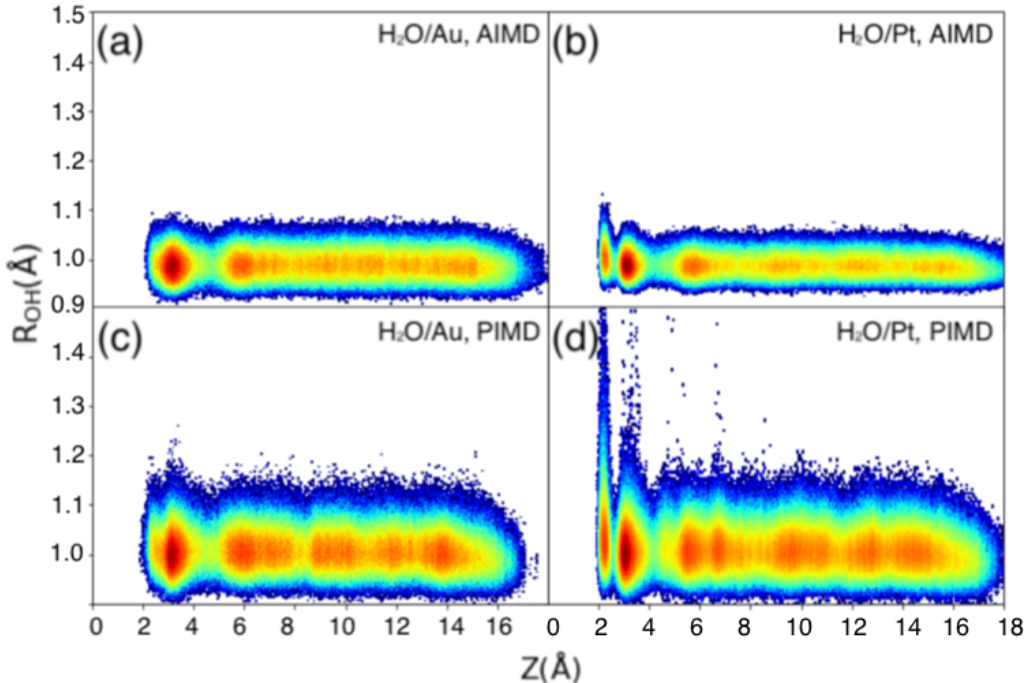

Supplementary Figure 6: Distribution of the intra-molecular OH bond length as obtained from AIMD(a,b) and (c,d) from PI-AIMD for water in contact with Au(left panel) and Pt(right panel). Distributions' colour code: from blue to red indicates an increased probability of finding the respective value. The distributions are obtained as averages over all OH and the whole trajectory.
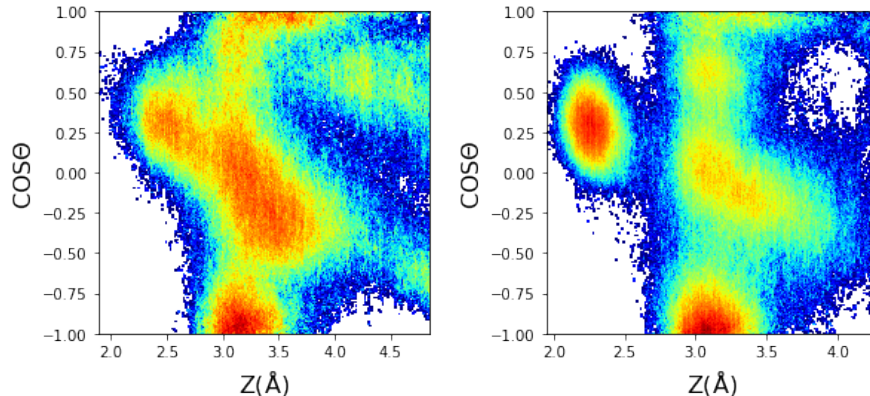
Supplementary Figure 7: Distribution of the cosine of the angle between OH and the surface normal, plotted as function of the height over the clean Au(111) (left) and Pt(111) surface (right). We only show results from the quantum sampling.

Electronic density of states calculations

The different interaction of water with the two considered metallic surface is rationalised in terms of the electronic structure at the interface. In FIG.8 we report projected density of states (PDOS) averaged on a selection of 25 snapshots extracted from both the classical and the quantum trajectories sampling the Pt/H_2O and the Au/H_2O systems. The PDOS calculations are carried out for each configuration, and each bead in the case of PI-AIMD, using the Fermi-Dirac distribution of the molecular orbitals' occupation, with a smearing temperature of 300 K. On Pt, we notice that the 1b1 band at about -3 eV is partially depleted at the interface, and there are water contributions to states across the Fermi energy, where the Pt-d band is still intense. This is an evidence of hybridisation between water and Pt states, with a partial charge transfer from the water towards the metal. This effect is less pronounced on gold, where, moreover, the intensity of the d-band at E_f is much lower. The water PDOS from the quantum snapshots is slightly broader than the classical one due to the delocalization of the hydrogens. Apart from this broadening, we observe that the electronic redistribution picture does not change between the classical and quantum sampling.
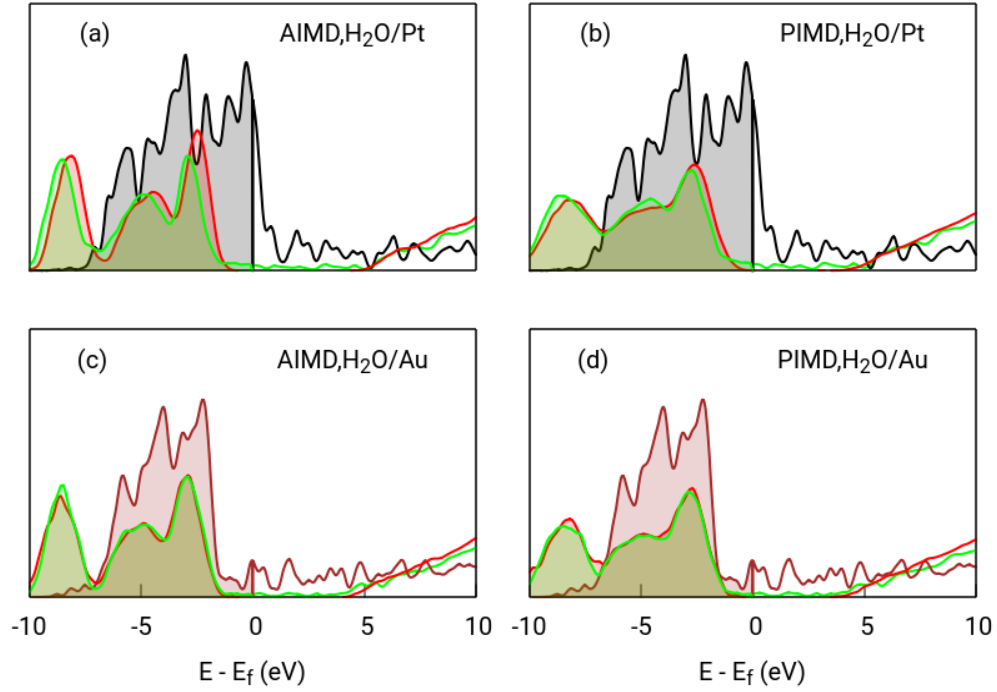
Supplementary Figure 8: Electronic density of states projected on the water molecules in the bulk (red), on the molecules at the interface (green), and the d-band of the metal (grey). a) and b) refer to the Pt(111)/H$_2$O system, sampled by classical and quantum dynamics, respectively. c) and d) are calculated from the classical and quantum sampling of Pt(111)/H$_2$O. The reference energy E_f corresponds to the Fermi level as computed at each extracted snapshot.

Hirshfeld population analysis

Based on Hirshfeld population analysis, the charge of oxygen atoms belonging to adsorbed water molecules and OH* species is about -0.65 e, while the oxygen in bulk water are about -1.24 e. The more positive oxygens at the interface suggest a partial electron transfer to platinum. The charge transfer between water and gold surface are instead less significant as indicated by the interface's oxygen charges of about -1.00 e.
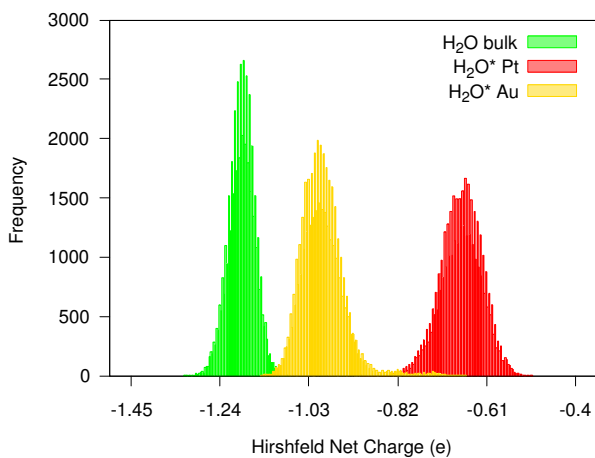

Supplementary Figure 9: Hirshfeld charge distribution of oxygen from bulk water (green) and interfacial water at platinum surface (red) and at gold surface (yellow)

Statistical errors in free energy evaluations

The error is estimated from

$$f_{\pm}(t) = \langle F(t) \rangle \pm \frac{a}{\sqrt{t}}$$

where $\langle F(t) \rangle$ is the time average of the free energy. The coefficient a is fitted such that 95% of the $F(t)$ is between $f_{+}(t)$ and $f_{-}(t)$. Hence, the statistical error is given as $\frac{a}{\sqrt{t}}$.
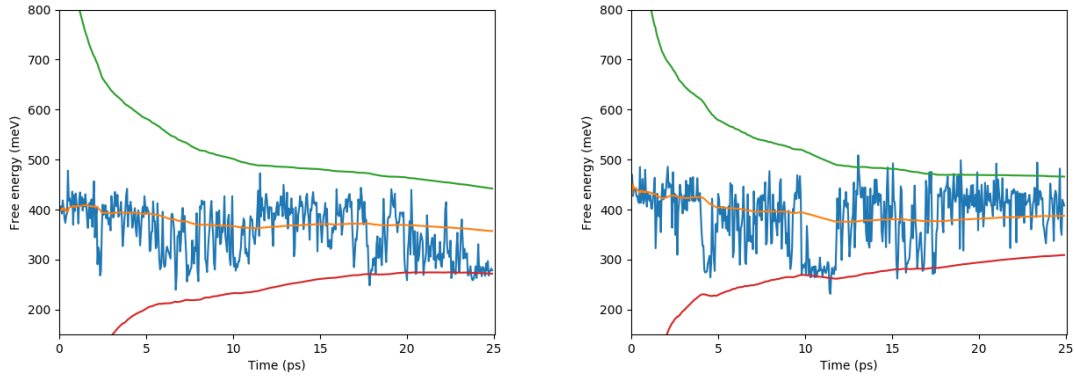
Supplementary Figure 10: Block average of $F(t)$ (blue), running average $\langle F(t) \rangle$ (orange), and $f_{\pm}$ (green and red) as obtained from the estimate of the statistical error. The left panel is obtained from the data collected from the H_2O simulations, right panel from the D_2O simulations. The block size of 50 fs has been used to calculate the free energy.

References

(1) Perdew, J. P.; Burke, K.; Ernzerhof, M. Generalized gradient approximation made simple. *Physical review letters* **1996**, *77*, 3865.

(2) Grimme, S.; Antony, J.; Ehrlich, S.; Krieg, H. A consistent and accurate ab initio parametrization of density functional dispersion correction (DFT-D) for the 94 elements H-Pu. *The Journal of chemical physics* **2010**, *132*, 154104.

(3) VandeVondele, J.; Krack, M.; Mohamed, F.; Parrinello, M.; Chassaing, T.; Hutter, J. Quickstep: Fast and accurate density functional calculations using a mixed Gaussian and plane waves approach. *Computer Physics Communications* **2005**, *167*, 103–128.

(4) VandeVondele, J.; Hutter, J. Gaussian basis sets for accurate calculations on molecular systems in gas and condensed phases. *The Journal of chemical physics* **2007**, *127*, 114105.

(5) Goedecker, S.; Teter, M.; Hutter, J. Separable dual-space Gaussian pseudopotentials. *Physical Review B* **1996**, *54*, 1703.

(6) Hartwigsen, C.; Gœdecker, S.; Hutter, J. Relativistic separable dual-space Gaussian pseudopotentials from H to Rn. *Physical Review B* **1998**, *58*, 3641.

(7) Bengtsson, L. Dipole correction for surface supercell calculations. *Physical Review B* **1999**, *59*, 12301.

(8) Ceriotti, M.; Markland, T. E. Efficient methods and practical guidelines for simulating isotope effects. *The Journal of chemical physics* **2013**, *138*, 014112.

(9) Ceriotti, M.; Fang, W.; Kusalik, P. G.; McKenzie, R. H.; Michaelides, A.; Morales, M. A.; Markland, T. E. Nuclear quantum effects in water and aqueous systems: Experiment, theory, and current challenges. *Chemical reviews* **2016**, *116*, 7529–7550.

(10) Bajaj, P.; Richardson, J. O.; Paesani, F. Ion-mediated hydrogen-bond rearrangement through tunnelling in the iodide–dihydrate complex. *Nature chemistry* **2019**, *11*, 367.